TU Delft

Research note

Challenges in adjoint-based well location optimization when using well models

Elham Ashoori and Jan Dirk Jansen

Department of Geoscience and Engineering, TU Delft

Version 1b, September 2015

Title:	**Challenges in adjoint-based well location optimization when using well models**
Version	1b
Author:	Elham Ashoori and Jan Dirk Jansen
Date:	September 2015
Type of report:	Research note
Organization:	Delft University of Technology Department of Geoscience and Engineering P.O. Box 5048 2600 GA Delft The Netherlands j.d.jansen@tudelft.nl
Keywords:	well location optimization, well model, adjoint, Ding
Changes:	Version 1a (January 2015): original version (unpublished) Version 1b (September 2015): corrected equation (4)

Abstract

There is a general consensus that the most efficient method for large-scale well location optimization is gradient-based with gradients computed with an adjoint formulation. Handels et al. (2007) (later published in journal form as Zandvliet et al., 2008), were the first to use the adjoint method for well placement optimization for which they introduced the concept of 'pseudo wells' surrounding the well to be optimized. Sarma et al. (2008) presented a method to determine the sensitivity of the objective function with respect to the actual well locations directly from the adjoint gradients. The direct dependency of the objective function on the well location comes from weighing the well indices of the pseudo wells by a continuous well-location-dependent function. However, this method is not consistent with the use of the Peaceman well-inflow model.

In this work we utilize the Ding well-inflow model (1994), which adjusts the transmissibilities of the adjacent grid blocks of off-centered wells. The basic underlying idea is that the explicit dependency of the flow equations on the well location, as formulated in the Ding model, would enable a direct calculation of the adjoint gradients of the objective function with respect to the well location. Unfortunately, attempts to implement this idea resulted in significant challenges. Using a simple homogenous 2-D reservoir example, we demonstrate how the non-smoothness of the objective function with the change in the well location, (resulting from assumptions in the Ding model) especially around the grid block borders can lead to incorrect adjoint gradients. We then show that this problem persists for a smoother objective function in which the Ding method is applied to a larger neighborhood around the well block.

We conclude that irregularities in the objective function resulting from the original Ding well-inflow model adversely affect gradient-based well location optimization and that modifications to the well model will be required to develop a robust Ding model-based well location optimization method.

Contents

Introduction

Determination of optimal well locations that maximize, e.g., the total oil production or net present value (NPV) over a given time period is of great importance throughout the life of a reservoir. For small reservoirs intuitive engineering judgment along with some numerical simulation may be sufficient to determine the proper well locations. However, if there are production constraints (e.g., pressure, rate, or water-cut constraints), predicting the optimal well locations intuitively may not be a trivial task, even for small reservoirs (Handels et al. 2007). For cases with a large number of wells computer-assisted optimization routines have the promise to result in much better results. Computer-assisted well location optimization routines can be divided into two major categories: gradient-based and gradient-free (stochastic) methods. A comprehensive review of the literature on well-placement-optimization methods is presented in Nasrabadi et al. (2012).

In principle, stochastic methods can be computationally imperative for large-scale problems and do not guarantee improvement within successive iterations. However, these methods are supposedly global in nature contrary to the gradient-based methods. The main invaluable gain of implementing a gradient-based method (with an associated adjoint model) over gradient-free methods is the reduction in the computational effort required. Nevertheless, a variety of gradient-free methods have been employed in literature to deal with the well-location optimization whereas the application of gradient-based methods to this optimization problem is limited to a few papers (Handels et al. 2007, Wang et al. 2007, Zandvliet et al. 2008, Sarma and Chen 2008, Castineira and Alpak, 2009, Zhang et al. 2010). The underlying reason is that the locations of wells are commonly defined by the well grid block indices in commercial simulators and, as a result, gradient-based methods cannot be used directly for such a discrete problem.

Handels et al. (2007) were the first to exploit the adjoint method for well placement optimization. In their method, eight pseudo-wells with very small rates are introduced in the centers of the grid blocks around the to-be-optimized wells. The adjoint gradient of the objective function with respect to the flow rate of each pseudo-well is then exploited as an indirect sign of the sensitivity of the objective function to the location of the well. Therefore, in each iteration step, the pseudo well with the largest gradient of the objective function averaged over the lifetime of the reservoir, is replaced by the respective to-be-optimized well until convergence is reached. The main limitation of this method, as implemented by Handels et al., is that the location of wells can only be updated to one of the locations of the eight pseudo-wells in each iteration, and thus, neither the search direction nor the step size are arbitrary.

Wang et al. (2007) also proposed an adjoint-based method for optimizing the location of injection wells but with a different optimization procedure than using pseudo wells. First, all grid blocks excluding the ones that accommodate the production wells are initialized by an injection well. Next, the conventional objective function is augmented by additional terms accounting for the cost of drilling the wells. The adjoint gradients are then defined as the gradients of the modified objective function with respect to the rates of these wells. If the rate of any of the wells goes to zero in the optimization iteration, that well is eliminated from the reservoir and its corresponding drilling cost are be removed from the modified objective function. By this method not only the location of the wells but also the number of the wells are optimized. However, in the optimization method presented by Wang et al. (2007), a

maximum of one well is removed in each optimization iteration. Later Zhang et al. (2010) employed the gradient projection method, which allowed for the elimination of more than one well in each iteration, to speed up the well-placement optimization algorithm.

The method of Sarma and Wen (2008) is the only attempt to determine the sensitivity of the objective function with respect to the actual well locations directly from the adjoint gradients. The direct dependency of the objective function on the well location comes from weighing the well indices of the pseudo wells by a continuous well-location-dependent function. The arbitrary location of the wells within each grid block in this method is an advantage over the methods, in which the well locations were restricted to the centers of grid blocks. However, the Sarma and Wen method is not consistent with the use of the Peaceman well inflow model because, in the Peaceman model it is assumed that wells are located in the grid block centers.

This work aims to address the well-placement optimization problem by deriving the adjoint gradients of the objective function directly with respect to the well locations. We utilize the Ding well inflow model (1994), which adjusts the transmissibilities of the adjacent grid blocks of off-centered wells as a function of the exact location of the wells. The explicit dependency of the well grid block transmissibilities on the well location in the governing system equations enables the direct calculation of the gradients of the objective function with respect to the well location by the adjoint method.

The rest of this report is organized as follows: First, the Ding well inflow model is briefly explained. Then, we describe in outline the adjoint method and how one can derive the adjoint gradients with respect to the well locations using the Ding model. The challenges we faced in implementing our proposed method on a simple homogenous 2-D reservoir example are discussed. We present the adjoint gradients for the case in which the Ding method is only applied to the well grid block. Finally, we repeat our experiment with the Ding well inflow model implemented to a larger neighborhood around the well grid block.

Ding well inflow model

Ding et al. (1994) proposed an approach based on the finite volume method, to better model the flow in the vicinity of wells and therefore improve the well inflow model. The main benefit of the Ding model over the conventional Peaceman well inflow model is its applicability to non-uniform Cartesian grids, non-Cartesian grids, non-fully-penetrating wells and off-centered wells (Ding et al., 1994). In the Ding approach, flow around the well is described through the analytical solution for near-well pressure corresponding to radial flow, which shows up in the model by the modified transmissibilities between the well block and its neighboring blocks. Therefore, the Ding model can be easily implemented in existing simulators by introducing a correction factor α as a multiplier for the conventional transmissibilities T_i for each of the grid blocks neighboring the well grid block:

$$T_i^{mod}\left(\boldsymbol{\xi}\right) = \alpha_i\left(\boldsymbol{\xi}\right) \times T_i \ , \tag{1}$$

where the subscript i denotes the grid block interface and where

$$\boldsymbol{\xi} = \begin{bmatrix} \xi_x \\ \xi_y \end{bmatrix} , \tag{2}$$

is a vector of local coordinates in the well grid block.

For an off-centered well located at (ξ_x, ξ_y), the α coefficient for each of the four well-block transmissibilities, depicted by the red rectangle in Figure 1, is a function of the well location through the angle θ formed by each well-block interface and the distance r between the well and each of the neighboring grid block centers:

$$\alpha_i(\xi) = \frac{\Delta x}{\Delta y} \frac{\theta_i(\xi)}{\ln\left(\frac{r_i(\xi)}{r_{eq}}\right)} \quad , \tag{3}$$

where Δx and Δy are the well block dimensions and r_{eq} is the Peaceman equivalent well block radius. The analytical solution for the flow around the well can be extended to another ring of grid blocks, shown by the red blocks in Figure 2. In this extended well model, called here the 'Two Ding ring model', 24 transmissibilities of the neighboring cells are modified. The four well block transmissibilities are modified with the aid of equation (3) while the rest of transmissibilities are modified by

$$\alpha_{ij}(\xi_x, \xi_y) = \frac{\Delta x}{\Delta y} \frac{\theta_{ij}(\xi)}{\ln\left(\frac{r_i(\xi)}{r_{0-i}(\xi)}\right)} \quad , \tag{4}$$

where the second subscript, j, refers to the grid block interface in the second ring (i.e. θ_{ij} is the angle between the radii from the well towards the endpoints of interface j of grid block i) and $r_{0\text{-}i}$ is the distance between the well grid block and the neighboring grid block i.

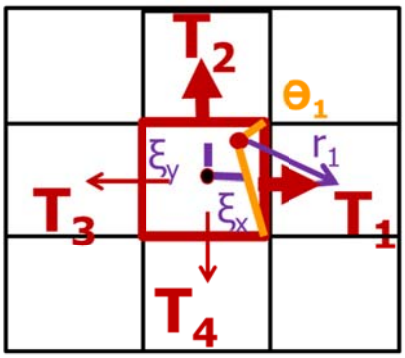

Figure 1: Schematic of flow from the well block to four adjacent grid blocks for a 'One Ding ring model'. The well is indicated by the red dot.

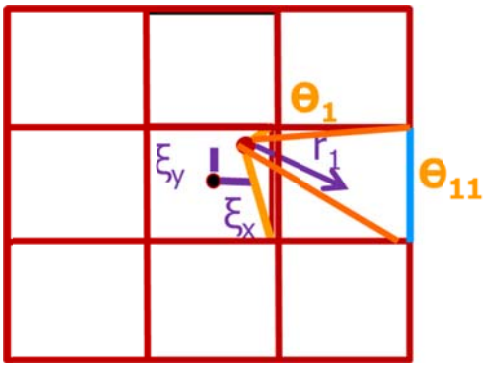

Figure 2: Schematic of flow from the well block to eight adjacent cells ('Two Ding ring model').

In principle, equation (3) can be used to extend the Ding model to more than two rings of cells around the well. For an *n*-well systems, with $n > 1$, however, flow is not radial anymore. Muskat (1937) shows that the pressure p around a configuration of n wells can be written as

$$p(x,y) = c + \frac{\mu q}{2\pi kh} \sum_{j=1}^{n} \ln r_j \ , \tag{5}$$

$$r_j = \sqrt{\left(x - x_j\right)^2 + \left(y - y_j\right)^2} \ , \tag{6}$$

where x and y are spatial coordinates, μ is viscosity, k is permeability, h is reservoir height and c is a constant. From this analytical pressure solution for an n-well system a new expression for the Ding multipliers can be obtained by the same method as for isolated wells (Ding and Renard, 1994). The following equations apply to the so-called first and second Ding rings, respectively:

$$\alpha_i(\xi) = \frac{\Delta x}{\Delta y} \frac{\sum_{k=1}^{n} \theta_{i,k}(\xi)}{\sum_{k=1}^{n} \ln\left(\frac{r_{i,k}(\xi)}{r_{eq}}\right)} \ , \tag{7}$$

$$\alpha_{ij}(\xi) = \frac{\Delta x}{\Delta y} \frac{\sum_{k=1}^{n} \theta_{ij,k}(\xi)}{\sum_{k=1}^{n} \ln\left(\frac{r_{i,k}(\xi)}{r_{0-i,k}(\xi)}\right)} \ , \tag{8}$$

where k is now the well counter.

Adjoint gradients

Adjoint models have been widely used, mostly for optimizing the operating conditions of wells (i.e., rates or bottom hole pressure), but have also found some applicability for well-location optimizations problem in reservoir engineering. A review of all previous work using adjoint models in reservoir simulation can be found in Jansen (2011). The main benefit of using the adjoint method is that regardless of the number of optimization variables, adjoint gradients can be obtained at a computational cost of about two simulation runs.

The well-location optimization problem in 2D requires the (x, y) location of all wells to be obtained, such that the objective function is maximized. In the following $\mathbf{z}$ represents a long vector of all well locations

$$\mathbf{z} = \begin{bmatrix} x_1 & y_1 & x_2 & y_2 & \cdots & x_N & y_N \end{bmatrix}^T , \tag{9}$$

where N is the total number of wells. Note that the final goal in practice is to optimize the well locations and the well rates (or bottom hole pressures) at the same time with the adjoint method (see, e.g., Forouzanfar 2010). However, in this work we focus only on optimizing the well locations with the given well operating conditions.

The mathematical formulation of this problem is as follows:

$$\max_{\mathbf{z}} J\left(\mathbf{u}_{1:K}, \mathbf{x}_{1:K}\right) , \tag{10}$$

subject to

$$\mathbf{g}_k\left(\mathbf{u}_k, \mathbf{x}_{k-1}, \mathbf{x}_k, \mathbf{z}\right) = \mathbf{0}, \quad k = 1, 2, \ldots, K , \tag{11}$$

$$\mathbf{x}_0 = \breve{\mathbf{x}}_0 , \tag{12}$$

where $\mathbf{g}$ is a system of nonlinear algebraic–differential system equations, $\mathbf{u}$ is a vector of input variables (i.e., total rates or bottom hole pressure of the wells), $\mathbf{x}$ is a vector of state variables (i.e., pressures and phase saturations in each grid block) and $\mathbf{x}_0$ is a vector of initial state variables, k is the time step counter and K the total number of simulation time steps. A colon is used to indicate a range of variables, e.g. $\mathbf{u}_{1:K}$ represents $\mathbf{u}_k, k = 1, 2, \ldots, K$. To simplify the notation we assume that control time steps coincide with simulation time steps, but this is not a fundamental restriction.

The main feature of the adjoint method is that it breaks the interdependency of all the variables (such as the dependency of $\mathbf{x}_k$ and on $\mathbf{x}_{k-1}$ and, through recursion, on all earlier instances of $\mathbf{x}$) by considering equations (8) and (9) as a set of additional constraints to the optimization problem, and applying the technique of Lagrange multipliers to solve the constrained optimization problem. Thus we adjoin the constraints to objective function to obtain an augmented objective function:

$$\bar{J}\left(\mathbf{u}_{1:K}, \mathbf{x}_{1:K}, \mathbf{z}\right) = \sum_{k=1}^{K}\left[J_k\left(\mathbf{u}_k, \mathbf{x}_k\right) + \boldsymbol{\lambda}_0^T(\mathbf{x}_0 - \breve{\mathbf{x}}_0)\delta_{k-1} + \boldsymbol{\lambda}_k^T \mathbf{g}_k\left(\mathbf{u}_k, \mathbf{x}_{k-1}, \mathbf{x}_k, \mathbf{z}\right)\right] , \tag{13}$$

where $\boldsymbol{\lambda}$ is a vector of Lagrange multipliers and where The Kronecker delta δ_{k-1} ensures that the initial condition constraint is included in the summation. The gradient of the objective function with respect to the controls (i.e. $\mathbf{u}_{1:K}$ for well control problem or $\mathbf{z}$ for the well location problem) can now be derived analytically; see Jansen (2011) or, for an alternative derivation, Kraaijevanger et al. (2007).

In this work we introduce this dependency by implementing the Ding well model in the system equations. In contrast, if we used the conventional Peaceman well model, the system equations and the objective function would not depend on the well coordinates, and thus, it would be impossible to derive the adjoint gradients with respect to the well locations directly. As noted in the previous section, grid block transmissibilities in the vicinity of the well blocks are corrected as a function of the exact well locations in the Ding well model. Therefore, applying the Ding model results in the system equations, and thus the objective

function, to be dependent on **z**. In the case where there is access to the system equations in the simulator, one can find the direct adjoint gradients of J with respect to the exact well locations **z** in the well grid blocks as:

$$\frac{\partial J}{\partial \mathbf{z}} = -\sum_{k=1}^{K} \boldsymbol{\lambda}_k^T \frac{\partial \mathbf{g}_k}{\partial \mathbf{z}} \ , \tag{14}$$

As mentioned, the system equations explicitly depend on the well locations through the grid-block transmissibilities T, once the Ding model is applied. For example, in the context of the SimSim simulator, the implicit Euler discretization of the system of equations (12) depends on the modified grid-block transmissibility matrix $\mathbf{T}^{mod}$ according to (see Appendix A for more details)

$$\mathbf{g}_k\left(\mathbf{x}_{k-1}, \mathbf{x}_k, \mathbf{z}\right) = \left(\hat{\mathbf{E}}_c\left(\mathbf{x}_k\right) - \Delta t \hat{\mathbf{A}}_c\left(\mathbf{x}_k, \mathbf{z}\right)\right)\mathbf{x}_k - \hat{\mathbf{E}}_c\left(\mathbf{x}_k\right)\mathbf{x}_{k-1} - \Delta t \hat{\mathbf{B}}_c\left(\mathbf{x}_k\right)\mathbf{u}_k \ , \tag{15}$$

where

$$\hat{\mathbf{A}}_c\left(\mathbf{x}_k, \mathbf{z}\right) = -\left(\mathbf{T}^{mod}\left(\mathbf{x}_k, \mathbf{z}\right) + \mathbf{F}\left(\mathbf{x}_k\right)\mathbf{J}\right) \ , \tag{16}$$

with the meaning of the various matrices explained in Appendix A. Substituting equation (16) into (15), we obtain the gradient of $\mathbf{g}_k$ with respect to **z** according to

$$\frac{\partial \mathbf{g}_k\left(\mathbf{x}_{k-1}, \mathbf{x}_k, \mathbf{z}\right)}{\partial \mathbf{z}} = \Delta t_k \frac{\partial \mathbf{T}^{mod}\left(\mathbf{x}_k, \mathbf{z}\right)}{\partial \mathbf{z}} \mathbf{x}_k \ , \tag{17}$$

Note that each element T_{ij}^m of the modified transmissibility matrix can be expressed as

$$T_{ij}^{mod}\left(\mathbf{x}_k, \mathbf{z}\right) = \alpha_{ij}\left(\mathbf{z}\right) T_{ij}\left(\mathbf{x}_k\right) \ , \tag{18}$$

such that

$$\frac{\partial T_{ij}^{mod}}{\partial z_m} = \frac{\partial \alpha_{ij}}{\partial z_m} T_{ij} \ . \tag{19}$$

Note that the subscripts i and j in α_{ij} have a different meaning than in equations (4) and (8). Once the dependency of the system equation on the well locations is derived, it can be substituted into equation (14) to find the direct gradient of the objective function with respect to the well locations.

Results

The purpose of this section is to present the objective function values and the adjoint gradients of objective function values with respect to the well locations for a simple reservoir once the Ding model is implemented in the SimSim simulator. The reservoir under consideration is a very simple 2D, oil/water reservoir that is 210×210×10 m in size, modeled by 21×21 grid blocks. The porosity is 0.3, the permeability is 0.5 Darcy and both are homogenous. The locations of four producers are fixed at the four corners whereas the location of the injector is to be optimized. The initial reservoir pressure is 40 MPa and the initial water saturation is 0.2. All the wells are set at constant bottom hole pressure (BHP) values of 40.3 MPa and 39.7 MPa for the injector and producer wells, respectively. The objective is to determine the optimal location of the injector such that net present value (NPV) is maximized over a period of 2 years according to the usual expression:

$$J = \sum_{k=1}^{K} \left[\frac{\sum_{j=1}^{N_{prod}} \left[r_o \times \left(q_{o,j} \right)_k - r_{wp} \times \left(q_{wp,j} \right)_k \right] - \sum_{i=1}^{N_{inj}} r_{wi} \times \left(q_{wi,i} \right)_k}{(1+b)^{\frac{t_k}{\tau_t}}} \Delta t_k \right], \quad (20)$$

where $q_{o,j}$ is the oil production rate of well j, $q_{wp,j}$ the water production rate of well j, $q_{wi,i}$ is the water injection rate of well i, r_o is the (constant) oil price, r_{wp} and r_{wi} are the (constant) water production and injection costs, Δt_k is the time interval of time step k in days, b is the discount rate for a reference time interval τ_t (which is usually taken as a year), and N_{inj} and N_{prod} are the number of injection wells and production wells respectively. For this study we used the following parameter values: r_o = 80 \$/bbl, r_{wp} = 5 \$/bbl, r_{wi}= 5 \$/bbl, b = 0.15 and τ_t = 365 d.

Trivially, for the symmetric homogenous reservoir in our example, the objective function is maximum if the injection well is located at the center. Figure 3 shows the NPV contours for a quarter of the homogenous reservoir. From now on, for the sake of brevity, all the figures show the results corresponding to the top-left quarter of the reservoir under study. The NPVs for each grid block are calculated by marching the injector well through 64 locations inside the cell as shown in the magnified square. For each well location (ξ_x, ξ_y), one can work out the Ding correction coefficients for the four transmissibilities of the grid block and employ the modified transmissibilities in the forward simulation run. As expected, the NPV gradually increases marching towards the center both in the x and y directions and appears to be quite smooth.

However, a wavy ripple behavior of the NPVs is more vivid in the non-contour plot as shown in Figure 4. This is the equivalent plot to the contour plot in Figure 3. Each curve represents NPVs if the injection well marches horizontally from the left border of the reservoir towards the center. For example, the first curve at the top shows the NPVs if the injection well marches from the top left corner of the reservoir to the top center. Likewise, the location of the injection well approaches vertically towards the center of the reservoir moving from the top curve towards the last bottom curve. The magnified figure depicts the NPVs for the two adjacent cells. Clearly, the non-smooth behavior becomes worse once the injection well approaches the cell borders as specified by yellow dots. This could be because the influence of the off-centered well on the flow distribution in the closer neighboring cells cannot simply be ignored.

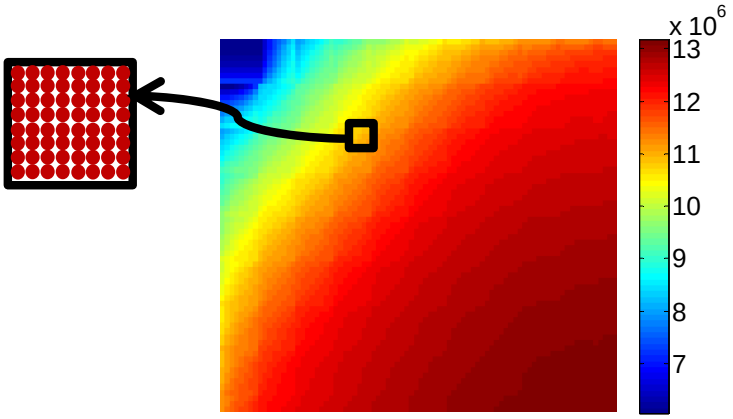

Figure 1: NPV contours for a quarter of a 2D, homogenous, oil/water reservoir for different injection-well locations and four producers fixed at the corners.

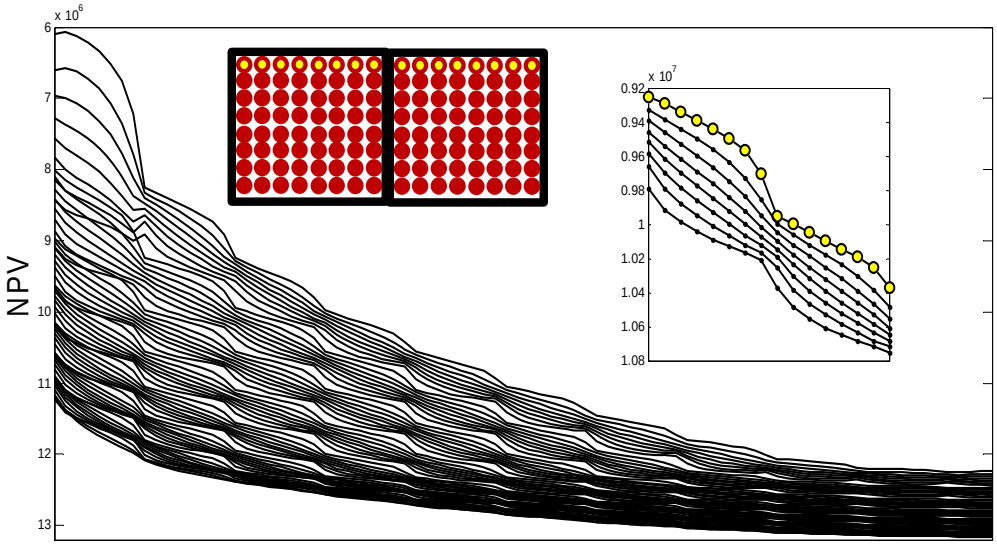

Figure 4. NPV curves corresponding to the contours in Figure 3. The location of the injection well approaches vertically towards the center of the reservoir moving from the top curve towards the last bottom curve.

As expected, the adjoint gradients of the objective function with respect to the well location do not exhibit a correct trend either. Figure 5 (top) shows the adjoint gradients of the objective function (corresponding to Figure 4) with respect to well location ξ_x (in red) and ξ_y (in blue) and Figure 5 (bottom) depicts the ratio of $\partial J / \partial \xi_y$ over $\partial J / \partial \xi_x$ (or $\partial \xi_y / \partial \xi_x$), respectively. Note that in this figure the gradients are shown for the injection well marching merely through the center of the grid blocks. For example, the first row of dots indicated by the purple arrow in the top plot correspond to the case where the injection well marches through the center of the grid blocks from the top left corner of the reservoir to the top center (shown by the horizontal arrow). For the simple reservoir studied, we expect that the objective function adjoint gradients in the x and y directions points towards the center of the reservoir. However, the gradients in Figure 5 become negative at some point close to the center of the reservoir in the y direction. We believe that as the injection well moves towards

the optimal location, and thereby the objective function becomes flatter, the bogus wavy behavior of the objective function dominates the slight change of the objective function resulting in the wrong negative gradients. Presumably, implementing the Ding model in a larger neighborhood of the well cell will improve the non-smoothness of the NPV contours and thus lead to more accurate gradients.

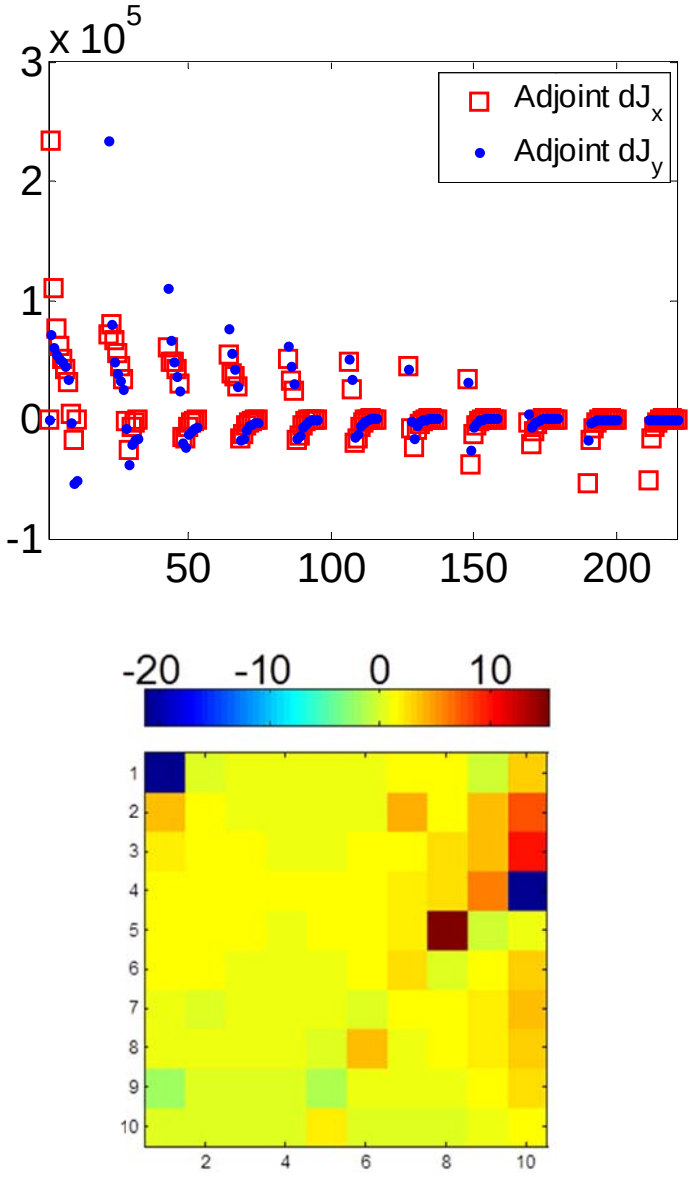

Figure 5: Top: adjoint gradients of the objective function (corresponding to Figure 4) with respect to well location ξ_x (in red) and ξ_y (in blue). Bottom: ratio $\partial J / \partial \xi_y$ over $\partial J / \partial \xi_x$ (or $\partial \xi_y / \partial \xi_x$). Note that in this figure the gradients are shown for the injection well marching merely through the center of the grid blocks.

Figure 6 exhibits the NPVs for the same case study as in Figure 4 with the only difference that the two-ring Ding model is implemented. However, we believe that extending the Ding model to a yet-bigger neighborhood may only minimally improve the results because the Ding transmissibility correction factors are already close to one for the second ring, as in the example shown in Figure 7. In this figure the off-centered well, shown by a red circle, is

located at (4.5 m, 4.5 m) from the central cell center, just 0.5 m away from the central-cell boundaries both in +x and +y directions.

According to Figure 8, implementing the two-ring Ding model results in a seemingly correct gradual decrease of $\partial J / \partial \xi$ both in the *x* and *y* directions as the injection well approaches the center of the reservoir. Obviously, the gradients have improved as compared to the case in which the conventional one-ring Ding model was implemented (see Figure 5). Knowing the optimal location of the injection well at the center of the homogenous reservoir, the ratio of $\partial J / \partial \xi_y$ over $\partial J / \partial \xi_x$ is expected to be greater than one if the well is located in the top triangle (shown in Figure 9) and less than one if otherwise. However, the results in Figure 9 do not demonstrate any logical trend.

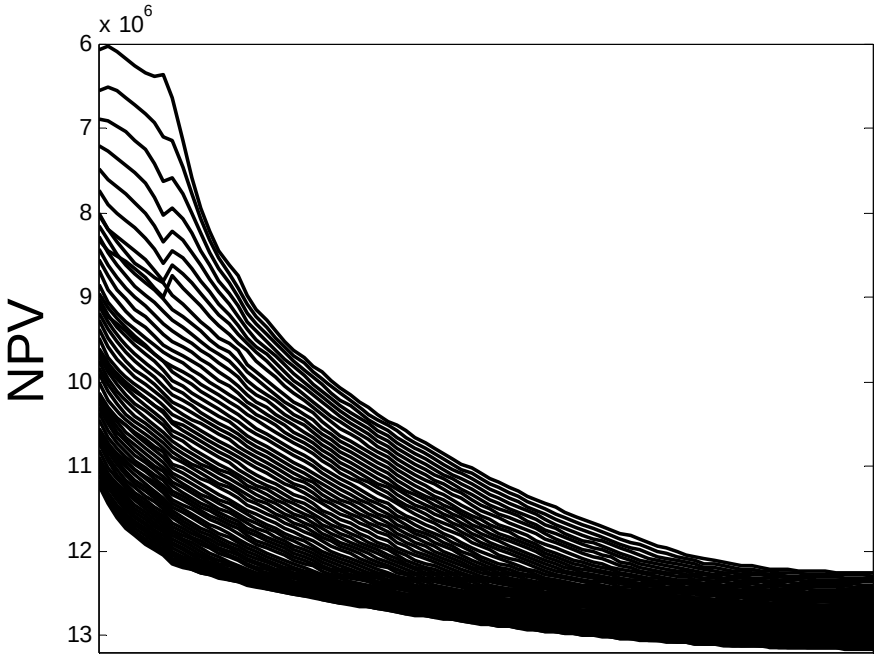

Figure 6: NPV curves with the same description as in Figure 4 except that the two-ring Ding model is implemented for this case.

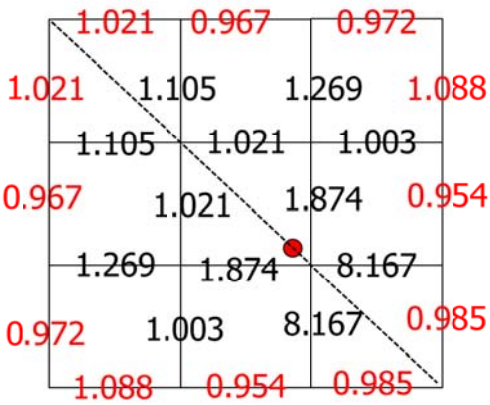

Figure 7: Ding correction factors for the 24 transmissibilities around an off-centered well, shown by a red circle, implementing the two-ring Ding model. The well is located at (4.5 m, 4.5 m) from the central cell center, just 0.5 m away from the central-cell boundaries both in the +x and +y directions.

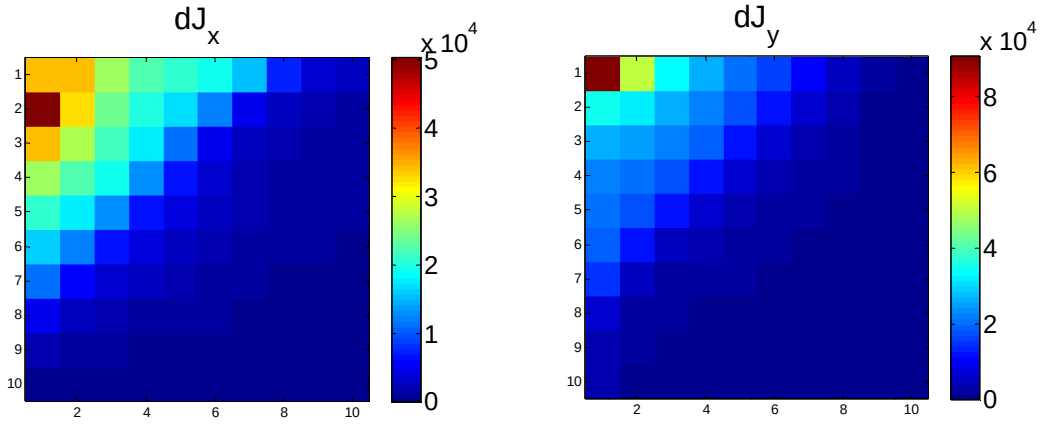

Figure 8. The adjoint gradients of the objective function (corresponding to Figure 6) with respect to well location ξ_x (right) and ξ_y (left) as the injection well marches through the center of the grids located on the top-left quarter of the reservoir under study.

To investigate the reason behind the erroneous adjoint gradients further, we study the approximate gradients of the objective function depicted in Figure 6 with respect to the well location. Figure 10 exhibits $\Delta J / \Delta \xi_x$ in red and $\Delta J / \Delta \xi_y$ in blue for the injection well marching along 8 rows (64 equally-spaced locations in each) within the purple rectangle. Clearly, the gradients are still unfavorably influenced by the cell borders although the two-ring Ding model is implemented and the objective function is quite smooth (see Figure 6). This implies that there is potentially a huge sensitivity of the gradient-based methods to even small irregularities of the objective function.

In addition, despite the expected relative change of the gradients in the two directions as the injection well moves location from left to right of the reservoir diagonal line, $\Delta J / \Delta \xi_x$ or $\Delta J / \Delta \xi_y$ may each dominate in magnitude depending on the exact location (row) of the injection well within the many grid-blocks. It should be noted, however, that in this work we have not corrected the Ding model to take into account the effect of reservoir boundaries, which undoubtfully may have caused the wrong behavior of the gradients. This needs to be

accounted for in any future work. Unfortunately, the bogus influence of the cell borders cannot be unresolved using this correction.

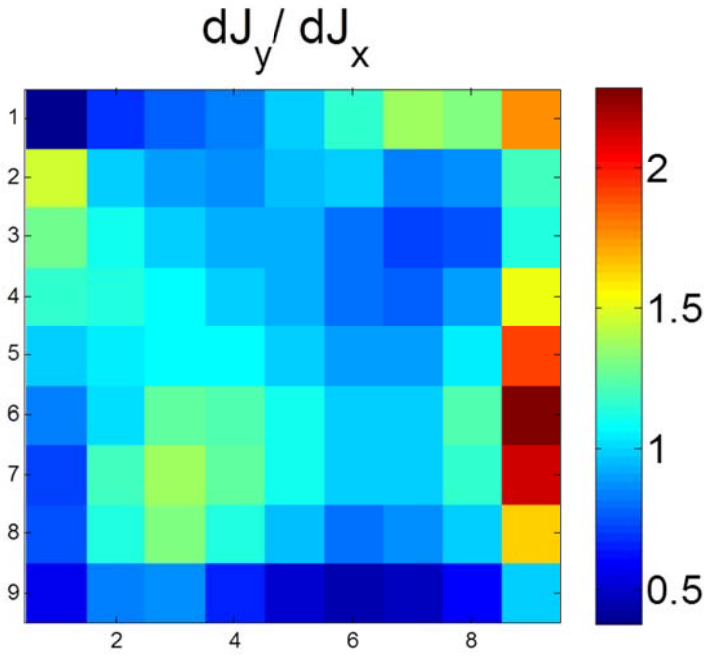

Figure 9. The ratio of $\partial J / \partial \xi_y$ over $\partial J / \partial \xi_x$ obtained from Figure 8.

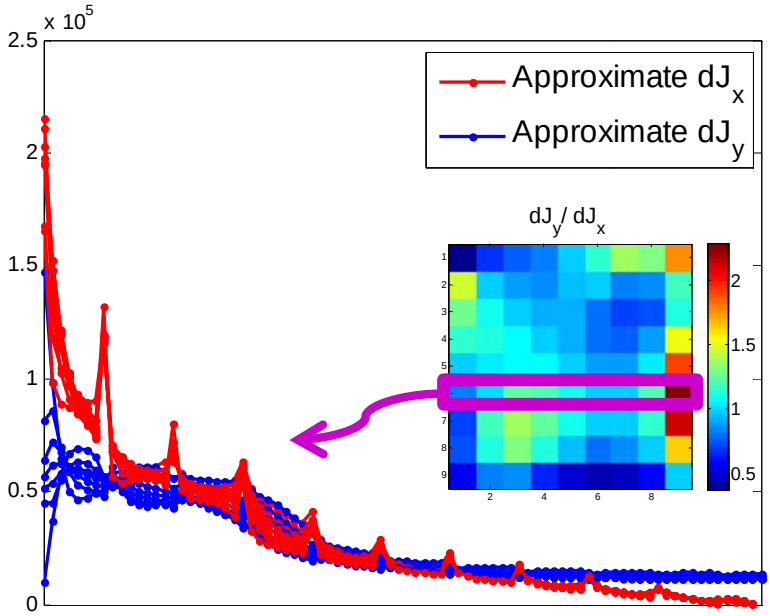

Figure 10. Approximate gradients $\Delta J / \Delta \xi_x$ in red and $\Delta J / \Delta \xi_y$ in blue, corresponding to Figure 6 for the injection well marching along 8 rows (64 equally-spaced locations in each) within the purple rectangle

Lastly, we also observed that the adjoint gradients are highly influenced by the forward simulator time step size. For example, the adjoint gradients behave inconsistently if the maximum allowed time step size is varied, unless a non-practically feasible step size is selected (e.g., in the order of 1-5 days for the presented case study). The reason for this is that the Newton-Raphson routine converges to a different objective-function value depending on

how close the initial guess is to the solution of our system equations. We suggest implementing the method proposed by Kourounis et al. (2014) in any future work to resolve the time-stepping issue.

Acknowledgements

This research was carried out within the context of the Recovery Factory program, a joint project of Shell Global Solutions International and Delft University of Technology.

References

Aziz, K. and Settari, A., 1979: *Petroleum reservoir simulation,* Applied Science Publishers, London.

Castineira, D., Alpak, F.O., 2009: Automatic well placement optimization in a channelized turbidite reservoir using adjoint based sensitivities. Paper SPE 119156, presented at the SPE Reservoir Simulation Symposium, The Woodlands, Texas, 2-4 February. DOI: 10.2118/119156-MS.

Ding, Y. and Renard, 1994: A new representation of wells in numerical reservoir simulation. *SPE Reservoir Engineering* **9** (2) 140-144. DOI: 10.2118/25248-PA.

Ding, Y., Renard, G., and Weill, L. 1998: Representation of wells in numerical reservoir simulation. *SPE Reservoir Engineering* **1** (1) 18-23. DOI: 10.2118/29123-PA.

Forouzanfar, F., Li, G., Reynolds, A.C., 2010: A two-stage well placement optimization method based on adjoint gradient. Paper SPE 135304 presented at the Annual Technical Conference and Exhibition, Florence, Italy, 19-22 September. DOI: 10.2118/135304-MS.

Handels, M., Zandvliet, M.J., Brouwer, D.R. and Jansen, J.D., 2007: Adjoint-based well placement optimization under production constraints. Paper SPE 105797 presented at the SPE Reservoir Simulation Symposium, The Woodlands, USA, 26-28 February. DOI: 10.2118/105797-MS.

Jansen, J.D., 2011: Adjoint-based optimization of multiphase flow through porous media – a review. *Computers and Fluids* **46** (1) 40-51. DOI: 10.1016/j.compfluid.2010.09.039.

Jansen, J.D., 2013: *A systems description of flow through porous media*. SpringerBriefs in Earth Sciences, Springer. ISBN: 978-3-319-00259-0 (print), 978-3-319-00260-6 (online). DOI: 10.1007/978-3-319-00260-6.

Kraaijevanger, J.F.B.M., Egberts, P.J.P., Valstar, J.R. and Buurman, H.W., 2007: Optimal waterflood design using the adjoint method. Paper SPE 105764 presented at the *SPE Reservoir Simulation Symposium*, Houston, USA, 26-28 February. DOI: 10.2118/105764-MS.

Kourounis, D., Durlofsky, L.J., Jansen, J.D. and Aziz, K., 2014: Adjoint formulation and constraint handling for gradient-based optimization of compositional reservoir flow. *Computational Geosciences* **18** (2) 117-137. DOI: 10.1007/s10596-013-9385-8.

Muskat, M., 1937: *The flow of homogeneous fluids through porous media*, McGraw-Hill, New York.

Nasrabadi, H., Morales, A., and Zhu, D. 2012: Well placement optimization: A survey with special focus on application for gas/gas-condensate reservoirs. *Journal of Natural Gas Science and Engineering*, **5**, 6-16. DOI: doi:10.1016/j.jngse.2011.10.002.

Sarma, P. and Chen, W.H., 2007: Efficient well placement optimization with gradient-based algorithms and adjoint models. Paper SPE 112257 presented at the SPE Intelligent Energy Conference and Exhibition, Amsterdam, The Netherlands, 25-27 February. DOI: 10.2118/112257-MS.

Wang, C., Li, G., and Reynolds, A.C., 2007: Optimal well placement for production optimization. Paper SPE 111154 presented at the SPE Eastern Regional Meeting, Lexington, USA, 17-19 October. DOI: 10.2118/111154-MS.

Zhang, K., Li, G., Reynolds, A.C., Yao, J., Zhang, L., 2010: Optimal well placement using an adjoint gradient. *Journal of Petroleum Science and Engineering* **73** (3-4) 220-226. DOI: 10.1016/j.petrol.2010.07.002.

Appendix A - State space formulation of two-phase porous media flow

Porous media flow

This Appendix presents a derivation of the equations for flow through porous media in state space form following closely Jansen (2013). As an example we consider two-phase (oil-water) isothermal, slightly compressible flow. Following the usual approach (see e.g. Aziz, and Settari, 1979) we can combine mass conservation equations and Darcy's law for each phase to obtain

$$-\nabla\cdot\left[\frac{\rho_i k_{ri}}{\mu_i}\mathbf{K}\left(\nabla p_i-\rho_i g\nabla d\right)\right]+\frac{\partial\left(\rho_i S_i\phi\right)}{\partial t}-\rho_i q_i'''=0\,, \tag{A.1}$$

where $\mathbf{K}$ is the permeability tensor, μ is fluid viscosity, k_r is relative permeability, p is pressure, g is acceleration of gravity, d is depth, ρ is fluid density, ϕ is porosity, S is fluid saturation, t is time, q''' is a source term expressed as flow rate per unit volume, and subscript $i\in\{o,w\}$ indicates the oil and water phases respectively. Equations (A.1) (one for each phase) contain four unknowns, p_w, p_o, S_w and S_o, two of which can be eliminated with aid of the relationships

$$S_w+S_o=1\ ,\quad p_o-p_w=p_c\left(S_w\right), \tag{A.2, A.3}$$

where $p_c(S_w)$ is the oil-water capillary pressure. Substituting equations (A.2) and (A.3) in equations (A.1), expanding the right-hand sides, applying chain-rule differentiation, and substituting isothermal oil, water and rock compressibilities

$$c_o=\frac{1}{\rho_o}\frac{\partial\rho_o}{\partial p_o}\bigg|_T\ ,\ c_w=\frac{1}{\rho_w}\frac{\partial\rho_w}{\partial p_w}\bigg|_T\approx\frac{1}{\rho_w}\frac{\partial\rho_w}{\partial p_o}\bigg|_T\ ,\ c_r=\frac{1}{\phi}\frac{\partial\phi}{\partial p_o}\,, \tag{A.4, A.5, A.6}$$

where T is temperature, allows us to express equations (A.1) in terms of p_o and S_w as follows:

$$-\nabla\cdot\left\{\frac{\rho_w k_{rw}}{\mu_w}\mathbf{K}\left[\left(\nabla p_o-\frac{\partial p_c}{\partial S_w}\nabla S_w\right)-\rho_w g\nabla d\right]\right\}+\rho_w\phi\left[S_w\left(c_w+c_r\right)\frac{\partial p_o}{\partial t}+\frac{\partial S_w}{\partial t}\right]-\rho_w q_w'''=0\,, \tag{A.7}$$

$$-\nabla\cdot\left[\frac{\rho_o k_{ro}}{\mu_o}\mathbf{K}\left(\nabla p_o-\rho_o g\nabla d\right)\right]+\rho_o\phi\left[\left(1-S_w\right)\left(c_o+c_r\right)\frac{\partial p_o}{\partial t}-\frac{\partial S_w}{\partial t}\right]-\rho_o q_o'''=0\,. \tag{A.8}$$

Equations (A.7) and (A.8) contain two state variables: the oil pressure p_o and the water saturation S_w. The equations are nonlinear because of the saturation dependency of the

capillary pressure p_c and the relative permeabilities k_{ro} and k_{rw}. In the more general case there may also be a pressure dependency of the densities ρ, the porosity ϕ, and the compressibilities c. In this paper we considered, without loss of generality, a simplified case where gravity and capillary forces can be neglected. After semi-discretization of the equations in space, e.g. with a finite difference or finite element procedure, we obtain the following system of nonlinear first-order differential equations,

$$\underbrace{\begin{bmatrix} \mathbf{V}_{wp}(\mathbf{s}) & \mathbf{V}_{ws} \\ \mathbf{V}_{op}(\mathbf{s}) & \mathbf{V}_{os} \end{bmatrix}}_{\mathbf{V}} \begin{bmatrix} \dot{\mathbf{p}} \\ \dot{\mathbf{s}} \end{bmatrix} + \underbrace{\begin{bmatrix} \mathbf{T}_w(\mathbf{s}) & \mathbf{0} \\ \mathbf{T}_o(\mathbf{s}) & \mathbf{0} \end{bmatrix}}_{\mathbf{T}} \begin{bmatrix} \mathbf{p} \\ \mathbf{s} \end{bmatrix} = \underbrace{\begin{bmatrix} \mathbf{F}_w(\mathbf{s}) \\ \mathbf{F}_o(\mathbf{s}) \end{bmatrix}}_{\mathbf{F}} \mathbf{q}_{well,t}, \tag{A.9}$$

where $\mathbf{p}$ and $\mathbf{s}$ are vectors of pressures p_o and water saturations S_w in the grid block centers, $\mathbf{V}$ is an accumulation matrix (with entries that are functions of the porosity ϕ, and the oil, water and rock compressibilities c_o, c_w and c_r), $\mathbf{T}$ is a transmissibility matrix (with entries that are functions of the rock permeabilities k, the oil and water relative permeabilities k_{ro} and k_{rw} and the oil and water viscosities μ_o and μ_w), $\mathbf{F}$ is a fractional flow matrix (with entries that have functional dependencies similar to those of $\mathbf{T}$), and $\mathbf{q}_{well,t}$ is a vector of total well flow rates with non-zero values in those elements that correspond to grid blocks penetrated by a well. The matrices $\mathbf{V}$, $\mathbf{T}$ and $\mathbf{F}$ are all functions of $\mathbf{s}$, either directly or through the parameters. In the more general case of high compressibility they are also a function of $\mathbf{p}$. The fractional flow matrices $\mathbf{F}_w$ and $\mathbf{F}_o$ are diagonal with fractional flows f_w and f_o as the elements that correspond to well grid blocks and zeros otherwise. In practice the source terms are often not the flow rates in the wells but rather the pressures. This can be accounted for by rewriting equation (A.9) in partitioned form as]

$$\left[\begin{array}{ccc|ccc} \mathbf{V}_{wp,11} & \mathbf{0} & \mathbf{0} & \mathbf{V}_{ws,11} & \mathbf{0} & \mathbf{0} \\ \mathbf{0} & \mathbf{V}_{wp,22} & \mathbf{0} & \mathbf{0} & \mathbf{V}_{ws,22} & \mathbf{0} \\ \mathbf{0} & \mathbf{0} & \mathbf{V}_{wp,33} & \mathbf{0} & \mathbf{0} & \mathbf{V}_{ws,33} \\ \hline \mathbf{V}_{op,11} & \mathbf{0} & \mathbf{0} & \mathbf{V}_{os,11} & \mathbf{0} & \mathbf{0} \\ \mathbf{0} & \mathbf{V}_{op,22} & \mathbf{0} & \mathbf{0} & \mathbf{V}_{os,22} & \mathbf{0} \\ \mathbf{0} & \mathbf{0} & \mathbf{V}_{op,33} & \mathbf{0} & \mathbf{0} & \mathbf{V}_{os,33} \end{array}\right] \left[\begin{array}{c} \dot{\mathbf{p}}_1 \\ \dot{\mathbf{p}}_2 \\ \dot{\mathbf{p}}_3 \\ \hline \dot{\mathbf{s}}_1 \\ \dot{\mathbf{s}}_2 \\ \dot{\mathbf{s}}_3 \end{array}\right] +$$

$$\left[\begin{array}{ccc|ccc} \mathbf{T}_{w,11} & \mathbf{T}_{w,12} & \mathbf{T}_{w,13} & \mathbf{0} & \mathbf{0} & \mathbf{0} \\ \mathbf{T}_{w,21} & \mathbf{T}_{w,22} & \mathbf{T}_{w,23} & \mathbf{0} & \mathbf{0} & \mathbf{0} \\ \mathbf{T}_{w,31} & \mathbf{T}_{w,32} & \mathbf{T}_{w,33} & \mathbf{0} & \mathbf{0} & \mathbf{0} \\ \hline \mathbf{T}_{o,11} & \mathbf{T}_{o,12} & \mathbf{T}_{o,13} & \mathbf{0} & \mathbf{0} & \mathbf{0} \\ \mathbf{T}_{o,21} & \mathbf{T}_{o,22} & \mathbf{T}_{o,23} & \mathbf{0} & \mathbf{0} & \mathbf{0} \\ \mathbf{T}_{o,31} & \mathbf{T}_{o,32} & \mathbf{T}_{o,33} & \mathbf{0} & \mathbf{0} & \mathbf{0} \end{array}\right] \left[\begin{array}{c} \mathbf{p}_1 \\ \mathbf{p}_2 \\ \mathbf{p}_3 \\ \hline \mathbf{s}_1 \\ \mathbf{s}_2 \\ \mathbf{s}_3 \end{array}\right] = \left[\begin{array}{ccc} \mathbf{0} & \mathbf{0} & \mathbf{0} \\ \mathbf{0} & \mathbf{F}_{w,22} & \mathbf{0} \\ \mathbf{0} & \mathbf{0} & \mathbf{F}_{w,33} \\ \hline \mathbf{0} & \mathbf{0} & \mathbf{0} \\ \mathbf{0} & \mathbf{F}_{o,22} & \mathbf{0} \\ \mathbf{0} & \mathbf{0} & \mathbf{F}_{o,33} \end{array}\right] \left[\begin{array}{c} \mathbf{0} \\ \breve{\mathbf{q}}_{well,t} \\ \mathbf{J}_3\left(\breve{\mathbf{p}}_{well} - \mathbf{p}_3\right) \end{array}\right]. \tag{A.10}$$

Here, the elements of vector $\mathbf{p}_1$ are the pressures in those grid blocks that are not penetrated by a well. The elements of $\mathbf{p}_2$ are the pressures in the blocks where the source terms are prescribed total well flow rates $\breve{\mathbf{q}}_{well,t}$, and those of $\mathbf{p}_3$ are the pressures in the blocks where the source terms are obtained through prescription of the bottom hole pressures $\breve{\mathbf{p}}_{well}$ with the aid of a diagonal matrix of well indices $\mathbf{J}_3$. To compute the oil and water flow rates in the wells with prescribed pressures we use the relationship

$$\begin{bmatrix} \bar{\mathbf{q}}_{well,w} \\ \bar{\mathbf{q}}_{well,o} \end{bmatrix} = \begin{bmatrix} \mathbf{F}_{w,33} \\ \mathbf{F}_{o,33} \end{bmatrix} \mathbf{J}_3 \left(\breve{\mathbf{p}}_{well} - \mathbf{p}_3 \right) \ . \tag{A.11}$$

To compute the bottom hole pressures $\bar{\mathbf{p}}_{well}$ in the wells with prescribed total flow rates we need an additional diagonal matrix $\mathbf{J}_2$ of well indices such that

$$\breve{\mathbf{q}}_{well,t} = \mathbf{J}_2 \left(\bar{\mathbf{p}}_{well} - \mathbf{p}_2 \right) \ , \tag{A.12}$$

from which we obtain

$$\bar{\mathbf{p}}_{well} = \mathbf{J}_2^{-1} \breve{\mathbf{q}}_{well,t} - \mathbf{p}_2 \ . \tag{A.13}$$

To bring these equations in state space form we define the *state vector* **x**, *input vector* **u** and *output vector* **y** as

$$\mathbf{u} \triangleq \begin{bmatrix} \breve{\mathbf{q}}_{well,t} \\ \breve{\mathbf{p}}_{well} \end{bmatrix}, \ \mathbf{x} \triangleq \begin{bmatrix} \mathbf{p} \\ \mathbf{s} \end{bmatrix} = \begin{bmatrix} \mathbf{p}_1 \\ \mathbf{p}_2 \\ \mathbf{p}_3 \\ \hline \mathbf{s}_1 \\ \mathbf{s}_2 \\ \mathbf{s}_3 \end{bmatrix}, \ \mathbf{y} \triangleq \begin{bmatrix} \bar{\mathbf{p}}_{well} \\ \bar{\mathbf{q}}_{well,w} \\ \bar{\mathbf{q}}_{well,o} \end{bmatrix} . \tag{A.14, A.15, A.16}$$

Equations (A.10), (A.11) and (A.13) can then be rewritten in nonlinear state space form

$$\dot{\mathbf{x}} = \mathbf{f}(\mathbf{x},\mathbf{u}) = \mathbf{A}_c(\mathbf{x})\mathbf{x} + \mathbf{B}_c(\mathbf{x})\mathbf{u} \ , \tag{A.17}$$

$$\mathbf{y} = \mathbf{h}(\mathbf{x},\mathbf{u}) = \mathbf{C}(\mathbf{x})\mathbf{x} + \mathbf{D}(\mathbf{x})\mathbf{u} \ , \tag{A.18}$$

where the state-dependent matrices $\mathbf{A}_c(\mathbf{x})$, $\mathbf{B}_c(\mathbf{x})$, $\mathbf{C}(\mathbf{x})$ and $\mathbf{D}(\mathbf{x})$ are defined as

$$\mathbf{A} \triangleq -\mathbf{V}^{-1} \underbrace{\left[\begin{array}{ccc|ccc} \mathbf{T}_{w,11} & \mathbf{T}_{w,12} & \mathbf{T}_{w,13} & \mathbf{0} & \mathbf{0} & \mathbf{0} \\ \mathbf{T}_{w,21} & \mathbf{T}_{w,22} & \mathbf{T}_{w,23} & \mathbf{0} & \mathbf{0} & \mathbf{0} \\ \mathbf{T}_{w,31} & \mathbf{T}_{w,32} & \mathbf{T}_{w,33} + \mathbf{F}_{w,33}\mathbf{J}_3 & \mathbf{0} & \mathbf{0} & \mathbf{0} \\ \hline \mathbf{T}_{o,11} & \mathbf{T}_{o,12} & \mathbf{T}_{o,13} & \mathbf{0} & \mathbf{0} & \mathbf{0} \\ \mathbf{T}_{o,21} & \mathbf{T}_{o,22} & \mathbf{T}_{o,23} & \mathbf{0} & \mathbf{0} & \mathbf{0} \\ \mathbf{T}_{o,31} & \mathbf{T}_{o,32} & \mathbf{T}_{o,33} + \mathbf{F}_{o,33}\mathbf{J}_3 & \mathbf{0} & \mathbf{0} & \mathbf{0} \end{array}\right]}_{-\hat{\mathbf{A}}}, \quad \mathbf{B} \triangleq \mathbf{V}^{-1} \underbrace{\left[\begin{array}{cc} \mathbf{0} & \mathbf{0} \\ \mathbf{F}_{w,22} & \mathbf{0} \\ \mathbf{0} & \mathbf{F}_{w,33}\mathbf{J}_3 \\ \hline \mathbf{0} & \mathbf{0} \\ \mathbf{F}_{o,22} & \mathbf{0} \\ \mathbf{0} & \mathbf{F}_{o,33}\mathbf{J}_3 \end{array}\right]}_{\hat{\mathbf{B}}},$$

$$\mathbf{C} \triangleq \left[\begin{array}{ccc|ccc} \mathbf{0} & \mathbf{I} & \mathbf{0} & \mathbf{0} & \mathbf{0} & \mathbf{0} \\ \mathbf{0} & \mathbf{0} & -\mathbf{F}_{w,33}\mathbf{J}_3 & \mathbf{0} & \mathbf{0} & \mathbf{0} \\ \mathbf{0} & \mathbf{0} & -\mathbf{F}_{o,33}\mathbf{J}_3 & \mathbf{0} & \mathbf{0} & \mathbf{0} \end{array}\right], \quad \mathbf{D} \triangleq \begin{bmatrix} \mathbf{J}_2^{-1} & \mathbf{0} \\ \mathbf{0} & \mathbf{F}_{w,33}\mathbf{J}_3 \\ \mathbf{0} & \mathbf{F}_{o,33}\mathbf{J}_3 \end{bmatrix}.$$

(A.19, A.20, A.21, A.22)

The equations are nonlinear because almost all elements of the matrices **V**, **T**, **F** and **J** are functions of the states **x**. The equations are *control affine* because they are linear in the controls **u**. In the systems and control literature $\mathbf{A}_c$ is usually called the *system matrix*, $\mathbf{B}_c$ the *input matrix*, **C** the *output matrix* and **D** the *direct throughput matrix*. These matrices are normally applied in a linear setting, i.e. they are not supposed to be functions of **x**. The

inverse of the accumulation matrix $\mathbf{V}$ as required in equations (A.19) and (A.20) can be computed at low computational costs because it consists of four diagonal sub matrices. However, we emphasize that there is no need to perform the inverse operation if the equations serve as a basis for computation, and that the explicit state space form (A.17) is only required for analysis of the system-theoretical properties of the equations. For computational purposes it is usually required to express the system equations in fully-implicit (residual) state-space form

$$\mathbf{g}\left(\mathbf{u},\mathbf{x},\dot{\mathbf{x}}\right)=\hat{\mathbf{E}}\dot{\mathbf{x}}-\hat{\mathbf{A}}\mathbf{x}-\hat{\mathbf{B}}\mathbf{u}=\mathbf{0}\ , \tag{A.23}$$

where $\hat{\mathbf{E}}=\mathbf{V}$ and where $\hat{\mathbf{A}}$ and $\hat{\mathbf{B}}$ are have been defined in equations (A.19) and (A.20).

Implicit Euler discretization

Consider the continuous-time state-space representation for two-phase flow with or without well model as given in equations (A.17) and (A.18):

$$\dot{\mathbf{x}}=\mathbf{A}_c\left(\mathbf{x}\right)\mathbf{x}+\mathbf{B}_c\left(\mathbf{x}\right)\mathbf{u}\ . \tag{A.24}$$

Here we have added subscripts c to indicate that the secant matrices $\mathbf{A}_c$ and $\mathbf{B}_c$ represent a continuous- time formulation. Applying implicit Euler discretization results in

$$\mathbf{x}_k=\mathbf{x}_{k-1}+\Delta t\mathbf{A}_c\left(\mathbf{x}_k\right)\mathbf{x}_k+\Delta t\mathbf{B}_c\left(\mathbf{x}_k\right)\mathbf{u}_k\ , \tag{A.25}$$

or, formally,

$$\mathbf{x}_k=\mathbf{A}_d\left(\mathbf{x}_k\right)\mathbf{x}_{k-1}+\mathbf{B}_d\left(\mathbf{x}_k\right)\mathbf{u}_k\ , \tag{A.26}$$

where

$$\mathbf{A}_d\left(\mathbf{x}_k\right)=\left[\mathbf{I}-\Delta t\mathbf{A}_c\left(\mathbf{x}_k\right)\right]^{-1},\quad \mathbf{B}_d\left(\mathbf{x}_k\right)=\Delta t\left[\mathbf{I}-\Delta t\mathbf{A}_c\left(\mathbf{x}_k\right)\right]^{-1}\mathbf{B}_c\left(\mathbf{x}_k\right)\ . \tag{A.27}$$

If we want to solve equation (A.26) using Newton-Raphson iteration, we could, formally, specify the implicit version of equation (A.26) in the form of a function $\mathbf{g}_k$ as

$$\mathbf{g}_k\left(\mathbf{u}_k,\mathbf{x}_{k-1},\mathbf{x}_k\right)=\mathbf{x}_k-\mathbf{A}_d\left(\mathbf{x}_k\right)\mathbf{x}_{k-1}-\mathbf{B}_d\left(\mathbf{x}_k\right)\mathbf{u}_k\ , \tag{A.28}$$

and work out the Jacobian $\partial\mathbf{g}_k/\partial\mathbf{x}_k$. In practice, it will be more convenient to start from the version with continuous-time matrices, as given in equation (A.25), such that $\mathbf{g}_k$ is expressed as:

$$\mathbf{g}_k\left(\mathbf{u}_k,\mathbf{x}_{k-1},\mathbf{x}_k\right)=\left(\mathbf{I}-\Delta t\mathbf{A}_c\left(\mathbf{x}_k\right)\right)\mathbf{x}_k-\mathbf{x}_{k-1}-\Delta t\mathbf{B}_c\left(\mathbf{x}_k\right)\mathbf{u}_k\ . \tag{A.29}$$

Moreover, it is usually computationally more efficient to use the generalized state-space formulation, which leads to

$$\mathbf{g}_k\left(\mathbf{u}_k,\mathbf{x}_{k-1},\mathbf{x}_k\right)=\left(\hat{\mathbf{E}}_c\left(\mathbf{x}_k\right)-\Delta t\hat{\mathbf{A}}_c\left(\mathbf{x}_k\right)\right)\mathbf{x}_k-\hat{\mathbf{E}}_c\left(\mathbf{x}_k\right)\mathbf{x}_{k-1}-\Delta t\hat{\mathbf{B}}_c\left(\mathbf{x}_k\right)\mathbf{u}_k\ . \tag{A.30}$$